Energy 68 (2014) 658–666

Contents lists available at ScienceDirect

Energy

journal homepage: www.elsevier.com/locate/energy

Experimental evaluation of a prototype thermoelectric system integrated with PCM (phase change material) for space cooling

Dongliang Zhao, Gang Tan*

University of Wyoming, Department of Civil and Architectural Engineering, 1000 E. University Avenue, Dept. 3295, Laramie, WY 82071, USA

A R T I C L E I N F O

Article history:
Received 21 October 2013
Received in revised form
19 January 2014
Accepted 25 January 2014
Available online 28 February 2014

Keywords:
Thermoelectric cooling
PCM
Heat storage
COP
Energy saving

A B S T R A C T

A prototype thermoelectric system integrated with PCM (phase change material) heat storage unit for space cooling has been introduced in this work. The PCM heat storage functions as cooling source and carries, partially at least, the cooling load during cooling operation. A simplified analytical model for the thermoelectric module has been adopted to investigate the theoretical performance characteristics of the modules. The experimental test in a reduced-scale chamber has achieved 7 °C temperature difference between "indoor" and "outdoor" environments and realized an average cooling COP (coefficient of performance) of 0.87 for the thermoelectric cooling system, with the maximum cooling COP of 1.22. Another comparison test for efficacy of PCM heat storage unit shows that 35.3% electrical energy has been saved from using PCM heat storage. During PCM charging (melting) process, natural convection has been observed playing a key effect factor of heat transfer in PCM.

1. Introduction

Thermoelectric cooling (or Peltier cooling) effect is the presence of cooling at the electrical junction of two different type conductors when electric current passing through and named after French physicist Jean Charles Athanase Peltier. Although this effect was discovered in the 19th century, it has long suffered from the inefficient thermoelectric material and was restricted to niche applications in areas including aerospace, military, medical and scientific research [1–4].

However, in fact, thermoelectric cooling has several advantages over their conventional counterparts such as compact in size and light in weight, high reliability, no mechanical moving parts and thus no noise, no working fluid so they are environmental friendly, and thermoelectric cooling can be powered by DC (direct current) which means easily integrating with PV (photovoltaic) panels, fuel cells and automobile DC electrical sources. At this stage, commercial applications of thermoelectric cooling are available for portable refrigerators, car seats and electronic cooling devices, but applying thermoelectric system to domestic space cooling remains much more challenging.

Gillott et al. [5] introduced thermoelectric cooling devices for small-scale space conditioning application in buildings. The unit assembled can generate up to 220 W of cooling power with a COP (coefficient of performance) of 0.46. Cheng et al. [6] developed a solar-driven thermoelectric cooling module for green building applications. The cooling module was able to produce a 16.2 °C temperature difference between the ambient and a $30 \times 12 \times 10$ cm^3 model house. He et al. [7] also studied a solar driven thermoelectric cooling system for a 0.125 m^3 model room. The minimum temperature achieved was 17 °C with COP of the thermoelectric device slightly higher than 0.45. Shen et al. [8] investigated a novel thermoelectric radiant air-conditioning system which employs thermoelectric modules as radiant panels instead of conventional hydronic panels. Miranda et al. [9] presented a feasibility study of thermoelectric air conditioner for electric vehicles. However, these investigates suffer from either low COP or economically unfeasible. Riffat and Qiu [10] compared the performances of thermoelectric and conventional vapor compression air-conditioners. Results showed that the actual COPs of vapor compression and thermoelectric air-conditioner were in the range of 2.6–3.0 and 0.38–0.45, respectively. Hermes and Barbosa [11] also concluded that thermodynamic efficiency of thermoelectric cooler was only 1% compared to 14% of Stirling and reciprocating vapor compression refrigeration systems.

It is critical to increase thermoelectric cooling system's COP for expanding their applications, which can be achieved by the thermal management techniques. Since the thermoelectric cooling system works like a heat pump, thus, removing heating/cooling energy generated at hot/cold sides promptly during the system operation

* Corresponding author. Tel.: +1 307 766 2017; fax: +1 307 766 2221.
E-mail address: gtan@uwyo.edu (G. Tan).

http://dx.doi.org/10.1016/j.energy.2014.01.090
0360-5442/Published by Elsevier Ltd.

Nomenclature

A	area, m^2
COP	coefficient of performance
f	thermoelectric module packing fraction covered by thermoelement
I	electric current, A
k	thermal conductivity, W/m K
K	thermal conductance, W/m^2 K
l	thermoelement height, m
$\dot{m}$	mass flow rate, kg/s
n	number of thermoelectric modules
N	number of thermocouples
P	electrical power, W
Q	energy, J
R	electrical resistance, Ω
T	temperature, °C
U	voltage, V
V	velocity, m/s

Greek symbols

α	Seebeck coefficient, V/K
Δt	time interval, s
ρ	electrical resistivity, Ω m

Subscripts

c	cold side
eff	effective
h	hot side
m	thermocouple
mod	module
max	maximum
t	total
unit	unit

period is of great importance. Compared to the cold side, thermal management in the thermoelectric hot side is more challenging because the heat flux at hot side is larger [12]. There exist two approaches to lower the hot side temperature. One approach is to use high performance heat sinks such as air cooled heat sink [13–15], water cooled heat sink [16,17], and heat pipes [18,19], while the other is to reduce the hot side HTF (heat transfer fluid, such as water or other coolant) temperature. Most researchers have been focused on the first approach, but there lacks of investigations on the latter one.

In this paper, experimental study of a prototype thermoelectric system integrated with PCM (phase change material) heat storage for space cooling is presented, where the PCM heat storage unit provides the thermoelectric cooling module's hot side with relatively lower temperature of heat transfer fluid (i.e. water). The purposes of this study are three folds: 1) to investigate how electric current and hot/cold side temperature difference affect the performance efficiency of the thermoelectric module; 2) to conduct thermoelectric cooling experiment for a reduced-scale model room (a 2.1 m^3 chamber); 3) to evaluate the effectiveness of PCM heat storage through experimental comparisons between different working modes.

2. Experimental apparatus and method

The tested integrated prototype thermoelectric cooling system primarily consists of a thermoelectric cooling unit, a shell-and-tube PCM heat storage unit, an air–water heat exchanger and the piping system as shown in Fig. 1. The thermoelectric cooling unit was installed inside a chamber that was located in a lab room. During experiments, the temperature-controllable lab room will model the ambient environment and the chamber will function as a conditioned space (i.e. the reduced-scale model room for cooling purpose). Due to lab room's temperature controllability, management of the cooling load in the chamber can be realized for comparison study. Heat released from the thermoelectric cooling unit can be pumped out through piping system with working fluid, that is, the hot side's heat transfer fluid (HTF), water here. This experimental system has the capability to run two operation modes, which are dissipating generated heat to outdoor air through the air–water heat exchanger (mode 1) and releasing heat to the shell-and-tube PCM heat storage unit (mode 2). These two modes can be easily switched over through manually controlling valves. Therefore, this experimental configuration provides the potential to investigate the thermoelectric cooling unit's performance under two operation modes for the same cooling load by maintaining the lab room temperature constant (i.e. within ±0.3 °C), while the ultimate heat sink is the outdoor air as the air–water heat exchanger was installed outside and the PCM heat storage unit, which would be discharged later using outdoor air. In Fig. 1, the *T* symbols are used to show the temperature measurements but each symbol may represent more than one temperature measuring point.

The schematic diagram and photo of the thermoelectric cooling unit are shown in Fig. 2. It is depicted that the thermoelectric module was sandwiched between the conductive fin and the water tank. Two axial fans were installed at the fin side to enhance convective heat transfer. In addition, a finned coil was employed in the water tank to achieve better heat exchange.

A schematic diagram and a photo of the shell-and-tube PCM heat storage unit are depicted in Figs. 3 and 4. The storage unit consists chiefly of a finned inner tube, an outer tube and a well-insulated rectangular shell envelope. The annulus space between inner tube and outer tube was filled with PCM. The inner tube was made of copper and has a size of 0.025 m inner diameter (i.d.) and 0.027 m outer diameter (o.d.), and the outer stainless steel tube has a size of 0.191 m (i.d.) and 0.203 m (o.d.). Sizes of the HTF water pipelines are the same as the inner tube. Lengths of the inner and outer tubes were both 1 m. During the charging (melting) process, PCM is initially in solid phase and heat transfer fluid (i.e. water) will flow through inside of the inner tube and exchange heat with PCM. When a charging process finishes, PCM will all convert into liquid phase. Throughout the charging process there is no noticeable heat exchange between the PCM heat storage unit and the lab room air because both the outer tube and the shell envelope were insulated. The discharging (solidifying) process is somehow like a reverse of the charging process, during which the outdoor air will be pushed by a fan, generally at night, to blowing through the space between outer tube and the rectangular shell envelope and PCM will thus be discharged.

The thermoelectric module used in this study was RC12-8. PCM used was RT22, which has a melting temperature of 19–23 °C (with main peak at 22 °C) and heat storage capacity of 200 kJ/kg. Detailed thermalphysical properties of the PCM are provided in Table 1. The HY3005D DC power supply device was used to provide direct

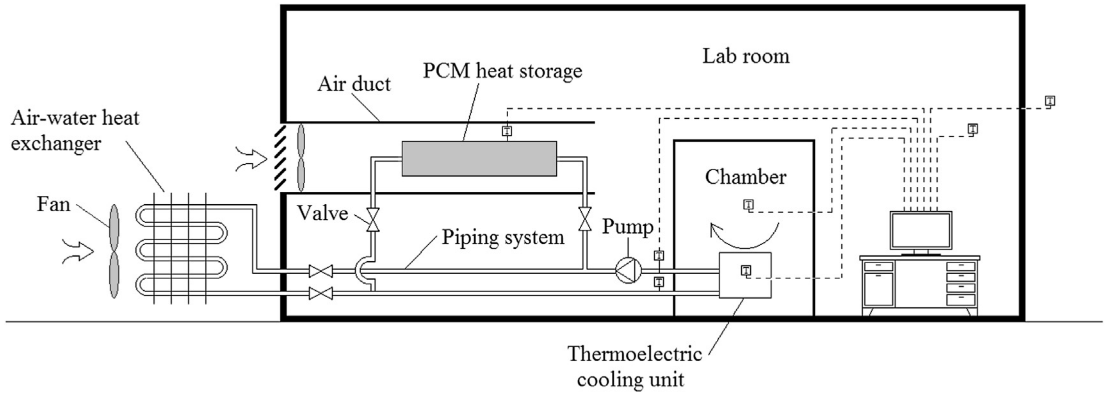

Fig. 1. Schematic diagram of the experimental setup for the prototype thermoelectric cooling system.

current power for thermoelectric modules. The chamber has a dimension of $1.2 \times 0.9 \times 1.9$ ($L \times W \times H$) m^3 with total volume of 2.1 m^3. The chamber wall was made of 5.1 cm thick extruded foam board with heat transfer coefficient of 0.568 W/m^2 K.

In operation, the prototype thermoelectric cooling system can switch between the two working modes based on outdoor air temperature conditions. For example, if outdoor air temperature is relatively low, such as in the early morning or late afternoon, the working mode 1 will be on operation and heat generated by space cooling will be dissipated to the outdoor environment. In contrast, when outdoor air temperature is high, the PCM heat storage unit will be activated and the system will operate in mode 2. At night, the PCM heat storage unit will be discharged through using relatively cool outdoor air. Therefore, PCM with appropriate melting temperature suitable for local weather conditions should be carefully selected in order to use "free cooling" at night for "re-generating" the PCM.

3. Mathematical modeling of the thermoelectric module and thermoelectric cooling unit

There are various modeling approaches for the thermoelectric modules including the simplified energy equilibrium model [5,7,8,17,20–22], numerical compact model [23], one-dimensional [24,25] and three-dimensional [26] modeling techniques with considerations of steady or transient states [27,28]. In general, more sophisticated models capture more characteristics in details but more modeling efforts and computing costs are needed.

In this study, to characterize the thermoelectric module's theoretical performance, a steady-state simplified energy equilibrium model has been applied in this study. The model is based on the assumption that thermalphysical properties of the thermoelectric material are temperature independent and Thomson effect is neglected. The heat absorbed at the cold side (Q_c) and released at the hot side (Q_h) is quantified by Eqs. (1) and (2), respectively.

$$Q_c = \alpha I T_c - 0.5 I^2 R - K(T_h - T_c) \tag{1}$$

$$Q_h = \alpha I T_h + 0.5 I^2 R - K(T_h - T_c) \tag{2}$$

where, α represents module Seebeck coefficient; I is electrical current; R denotes module electrical resistance; K is module thermal conductance; T_h and T_c are temperatures at module hot and cold sides, respectively.

Electrical power input (P_{mod}) of the thermoelectric module is:

$$P_{mod} = I^2 R + \alpha I (T_h - T_c) \tag{3}$$

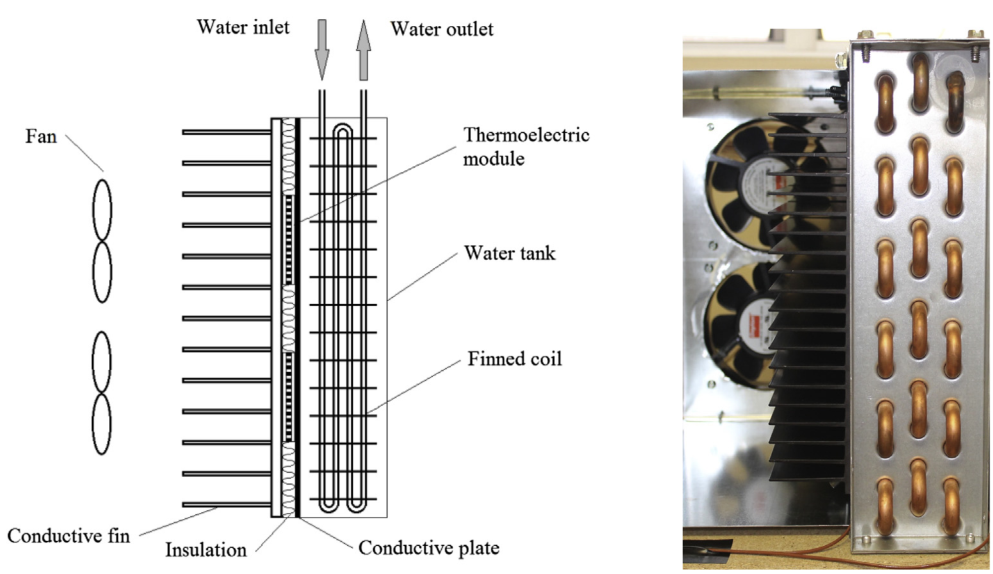

Fig. 2. Schematic diagram and photograph of the thermoelectric cooling unit.

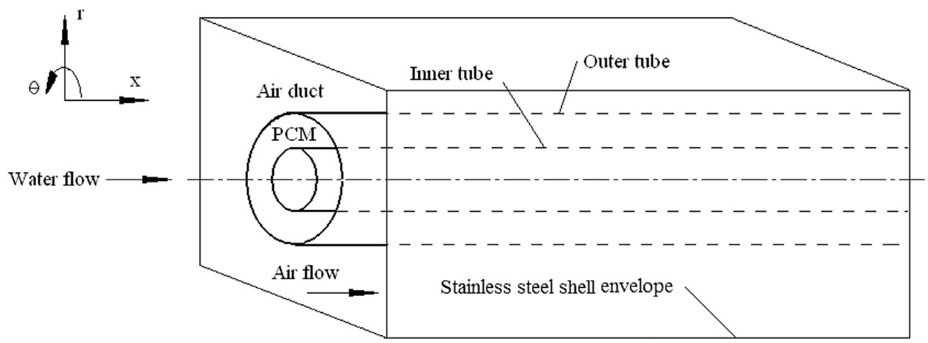

Fig. 3. Schematic diagram of the PCM heat storage unit.

Fig. 4. Photograph of the PCM heat storage unit during charging process.

Thus the theoretical cooling COP (COP_{mod}) of the thermoelectric module is then derived as:

$$COP_{mod} = \frac{Q_c}{P_{mod}} \tag{4}$$

The module electrical resistance (R) and thermal conductance (K) can be computed from material electrical resistivity (ρ) and thermal conductivity (k) from Eqs. (5) and (6). The module Seebeck coefficient is derived from Eq. (7)

$$R = \frac{4N^2 l\rho}{Af} \tag{5}$$

$$K = k\frac{Af}{l} \tag{6}$$

$$\alpha = N\alpha_m \tag{7}$$

where, N is the number of thermocouples in a thermoelectric module; A is the uniform cross-section area of the module; l is the thermoelement height; α_m is Seebeck coefficient of a thermocouple with the assumption that p-type and n-type thermoelements have the same Seebeck coefficient except opposite direction; and f is the packing fraction covered by thermoelement.

However, the thermoelectric module manufacturers generally would not provide material thermalphysical properties such as thermocouple Seebeck coefficient (α_m), thermal conductivity (k) and electrical resistivity (ρ). Chen and Snyder [23] developed a method using operation parameters Q_{max}, ΔT_{max}, and I_{max} to interpret out material thermalphysical properties as shown from Eqs. (8)–(10). Table 2 shows the technical specifications of RC12-8 that is adopted as thermoelectric modules for the prototype thermoelectric cooling system in this study.

$$\alpha_m = \frac{Q_{max}(T_h - \Delta T_{max})}{NT_h^2 I_{max}} \tag{8}$$

$$\rho = \frac{Af(T_h - \Delta T_{max})^2}{2T_h^2 l}\frac{Q_{max}}{N^2 I_{max}^2} \tag{9}$$

$$k = \frac{l(T_h - \Delta T_{max})^2}{AfT_h^2}\frac{Q_{max}}{\Delta T_{max}} \tag{10}$$

From air side, the thermoelectric cooling unit's cooling capacity

Table 1
Thermophysical properties of the PCM RT22 used in this research.

Property	RT22
Melting temperature (°C)	19–23 (main peak: 22)
Heat storage capacity (kJ/kg)	200
Density (kg/m^3)	880 (solid), 770 (liquid)
Thermal conductivity (W/m K)	0.2
Total volume (L)	18.7
Total mass (kg)	~15.4

Table 2
Technical specifications of RC12-8 (hot side temperature at 300 K) [29].

Item	Properties
Dimensions ($L \times W \times H$, mm)	40 × 40 × 3.5
Q_{max} (W)	71
I_{max} (A)	7.4
U_{max} (V)	14.7
ΔT_{max} (°C)	66
ZT factor	0.74

(Q_{unit}) can be evaluated and the unit's COP (COP_{unit}) is thus defined, by the following equations:

$$Q_{unit} = C_{p,air}\dot{m}(T_{in,air} - T_{out,air}) \quad (11)$$

$$COP_{unit} = \frac{Q_{unit}}{nP_{mod}} \quad (12)$$

where, $\dot{m}$, $T_{in,\ air}$ and $T_{out,\ air}$ are the mass flow rate, inlet and outlet temperatures of the air stream passing through the cooling unit, respectively.

The analytical modeling results for the thermoelectric module's cooling COP and cooling capacity are shown in Figs. 5 and 6, respectively. The module was evaluated at hot side temperature fixed at 300 K. Fig. 5 gives that for each given hot/cold side temperature difference (ΔT), there exists an optimum electric current leading to maximum cooling COP, and the optimum current increases with increasing ΔT. For each curve, the cooling COP first increases and then decreases with increasing electric current because large electric current will generate more Joule heat which will offset the Peltier cooling effect. As electric current increases, Joule heat will gradually dominate and thus these curves demonstrated a converging trend. Fig. 6 shows that the thermoelectric module's cooling capacity increases with electric current increasing, and also increases with the temperature difference decreasing. However, the cooling capacity definitely will not increase to infinite as the curve will turn to a convex shape when electric current continually increases. Huang [30] and Wang's [31] research on thermoelectric module's performance presented almost the same results as shown here but using a more detailed and heat-electricity coupled modeling approach.

4. Results and discussion

As shown in Figs. 5 and 6, the thermoelectric module's high cooling COP usually corresponds to low cooling capacity and high cooling capacity occurs with low cooling COP. Therefore, thermoelectric cooling system's optimization process is basically to find a best balanced point for both cooling capacity and COP. For the thermoelectric modules used in this study, the hot/cold side temperature difference ΔT will fall within the range of 10–15 °C due to space cooling application, which results in, from Figs. 5 and 6, a maximum theoretical module COP of 1.5–2.0 and corresponding

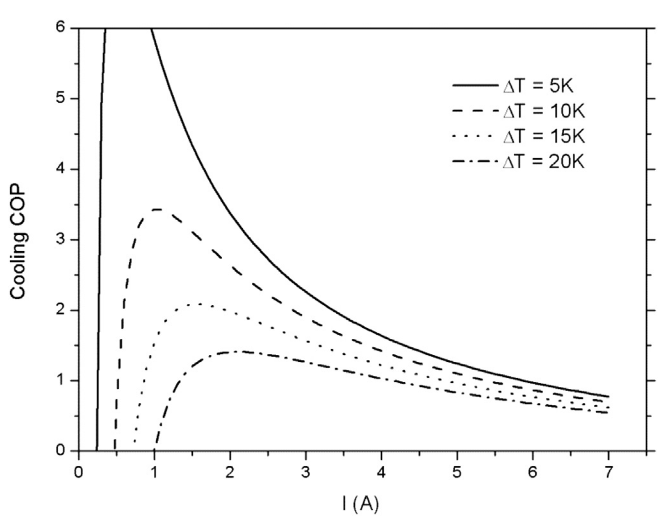

Fig. 5. Thermoelectric module's cooling COP versus electric current at different hot/cold side ΔT ($T_h = 300$ K).

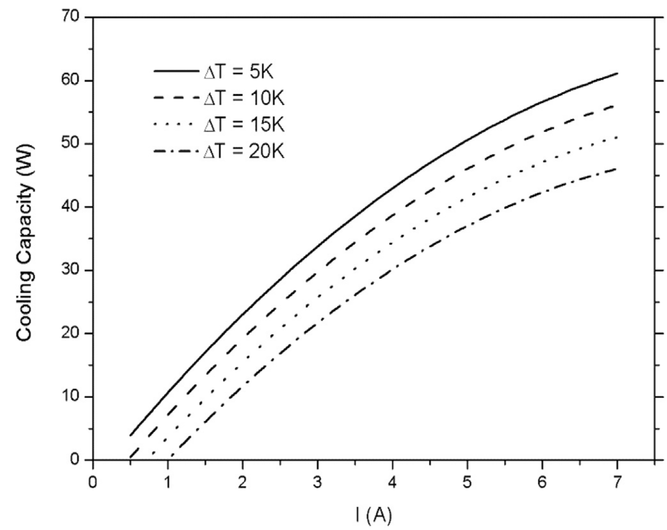

Fig. 6. Thermoelectric module's cooling capacity versus electric current at different hot/cold side ΔT ($T_h = 300$ K).

cooling capacity of 15–20 W for each module at an electric current of 1.5–2.1 A. The experiment in this work adopted electric current 2.5 A in order to approach slightly greater cooling capacity but still have high COP values. Total 15 thermoelectric modules have been used in this experimental study with electrical connection in parallel to achieve theoretically 225–300 W cooling capacity. During operation, the mass flow rate of HTF water through the inner tube was maintained constant and was 0.065 kg/s.

4.1. Performance study of the thermoelectric cooling system using PCM as heat storage

Experimental tests for the thermoelectric cooling system have been carried out in the Architectural Engineering research facility located at the University of Wyoming, Laramie, WY, USA. In the experiment to study the thermoelectric cooling system's performance characteristics, the air temperature of the lab room, which was modeling the outdoor environment, was maintained at 30 °C (see Fig. 1) and the PCM initial temperature was set to approximately 21 °C on average.

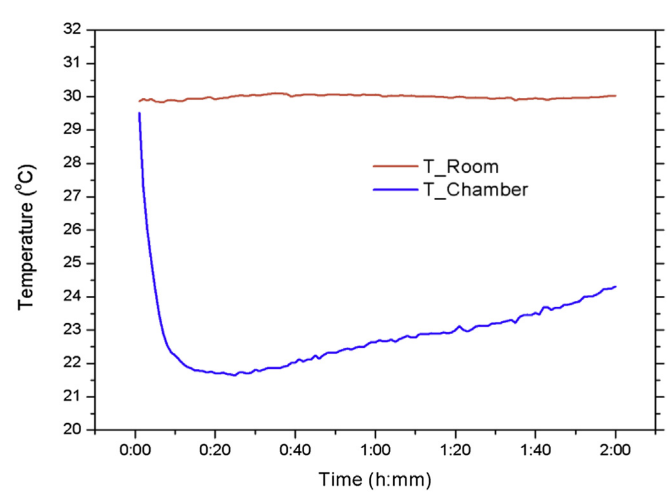

Fig. 7. Air temperature variations in the lab room and the chamber during the cooling process.

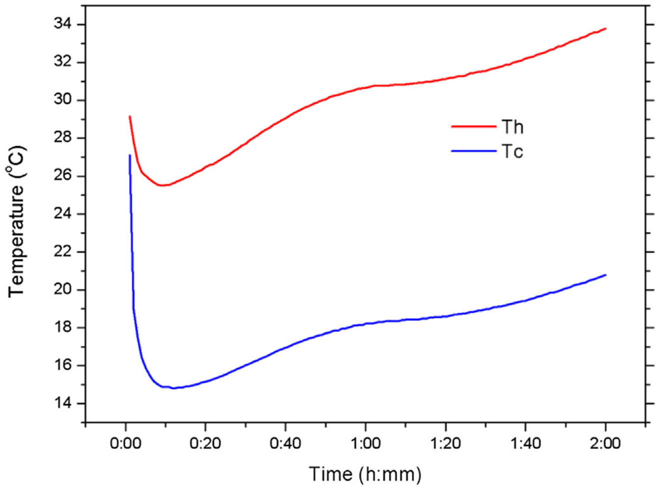

Fig. 8. Thermoelectric module's hot and cold side temperatures throughout the experimental test.

Fig. 7 gives the air temperature variations in the lab room and the chamber for a 2-h experiment period. The chamber air temperature dropped down very fast at the beginning 10 min to below 22 °C. Since then, the chamber air temperature rose gradually. The overall average air temperature in the chamber for the entire 2-h period was approximately 23 °C, 7 °C lower than the lab room air temperature. Thermoelectric module hot and cold sides' temperatures are shown in Fig. 8. Except the 10-min beginning period, the temperature difference between hot and cold sides was maintained at a relatively steady level, slightly increasing from 11 °C to 13 °C. Though input electric current is unchanged, the increase of hot/cold side temperature difference will lead to increasing electrical energy consumption as shown by Eq. (3), because larger temperature difference made it harder to "pump" heat from the cold side to the hot side.

The cooling COP was calculated using Eq. (12). Variation of the cooling COP and cooling capacity is depicted in Fig. 9, which shows that the maximum cooling COP value of 1.22 was achieved at the 10-min operation point. The overall average cooling COP for the entire experiment was 0.87. The cooling capacity has shown almost the same trend as the cooling COP and the maximum cooling capacity achieved was 210 W. The cooling capacity and COP decreased

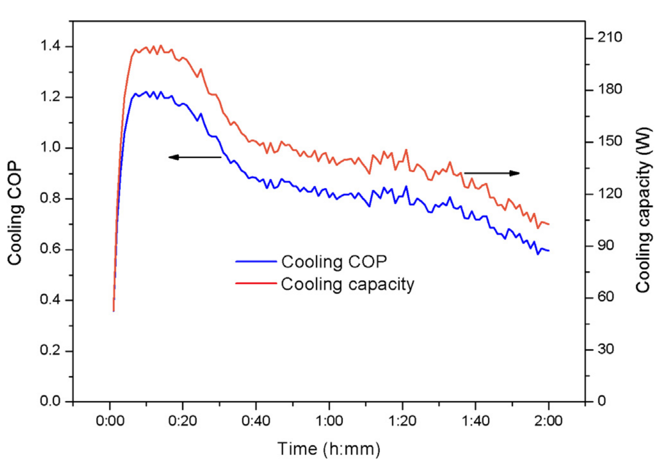

Fig. 9. The thermoelectric system's cooling COP and cooling capacity variations throughout the experimental test.

with experiment moving on because PCM temperature was increasing when more heat was released from the thermoelectric cooling unit to PCM, leading to thermoelectric unit's hot side temperature rising.

Both cooling COP (1.22) and cooling capacity (210 W) from the experiment were lower than the values from analytical modeling, which is mainly because thermal resistances at the thermoelectric module hot/cold sides lead to the cooling performance reduction. Comparison to some previous thermoelectric cooling studies is listed in Table 3.

During this PCM charging (melting) process, HTF water carried heat from the thermoelectric cooling unit to pass through the PCM heat storage unit, where water temperature decreased and PCM melted. Three thermocouples were placed into PCM to record PCM temperature changes and their locations are shown by black dots in Fig. 10, named lower, medium, and upper according to their positions along radius direction.

PCM temperature variations at these three points are depicted in Fig. 11, from which the PCM charging (melting) process may be divided into three stages. The first stage (pre-melting stage) was approximately from time 0:00 to time 0:40 (40 min in length), where heat conduction dominated the heat transfer within PCM because PCM was mainly in solid phase. During this stage, PCM temperature at the lower thermocouple location increased faster than temperatures at the other two because the lower one was located closer to the inner tube. Also, these three curves show the initial temperatures of PCM were not uniform and had temperature stratification caused by the discharging (solidifying) process, but the PCM average temperature was about 21 °C. The second stage (melting stage) was approximately from time 0:40 to time 1:10 (30 min in length). When PCM near the inner tube region has melted, a coexisting phenomenon of melted liquid phase and non-melted solid phase PCM would occur, with the melting interface gradually approaching towards a larger radius. Then, natural convection was generated in the liquid region caused by buoyancy force. Both heat conduction and natural convection worked for heat transfer within PCM. Three dashed lines (A, B, and C) in Fig. 11 indicate the approximate melting moments for PCM located at the lower, medium, and upper points, respectively. Once the upper layer of PCM started melting, the entire region of PCM was converted into liquid phase while the temperature difference between the lower layer and the upper layer was great, about 7 °C, which triggered natural convection within the melted PCM. The natural convection was so strong that a mixing effect can be observed from Fig. 11: the medium and upper points melted almost simultaneously and lower point even experienced a temperature drop at time 1:05. These phenomena would not happen if heat conduction has dominated heat transfer. The third stage (post-melting stage) was from time 1:10 to time 2:00 (50 min in length). After PCM at all three thermocouple locations melted, heat conduction would dominate heat transfer again because all three temperatures increased gradually in parallel and there was no mixing effect observed. In this stage, natural convection effect became small as the temperature difference within the PCM was small. The reason

Table 3
Comparison with some previous thermoelectric cooling researches.

Modules	Operation current (A)	Cooling capacity (W)	COP	Reference
Eight pieces UT8-12-40-RTV	4.8	220	0.46	[5]
One piece 127-03	–	~20	0.45	[7]
One piece TEC1-12706	1.2	<5	1.77	[8]
Two pieces 6L	~2.8	20	0.45	[18]
Fifteen pieces RC12-8	2.5	165	0.87	This work

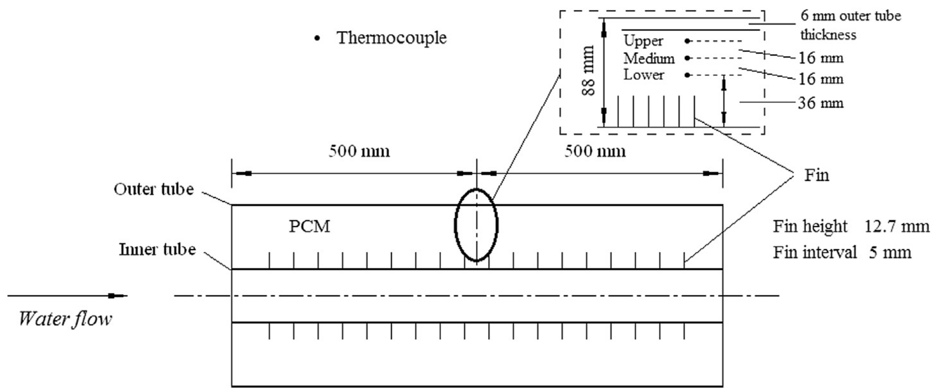

Fig. 10. Temperature measuring points (thermocouples) inside the PCM heat storage unit.

of the lower point temperature increasing slightly faster in the third stage than that in the first stage mainly attributes to that liquid PCM's thermal conductivity is greater than solid PCM's thermal conductivity. Fig. 11 also shows inlet and outlet temperature variations for the PCM heat storage unit's HTF water. With progress of the experiment the temperature difference between inlet and outlet HTF water gradually reduced from 2.1 °C at the beginning to 0.5 °C in the end.

Experiment of discharging (solidifying) process took place at night after outside air temperature dropped down. In this experiment, we conducted an 11-h discharging test that started from 8:30pm and continued to the next morning as shown in Fig. 12. During the discharging process, PCM's average temperature reduced from 33.6 °C to 17.5 °C. All three measured PCM temperatures changed in almost the same tendency. The upper point temperature was the lowest one because it was the closest to the heat transfer fluid (i.e. air). For each PCM temperature, there was a turning point at around 22 °C, which clearly indicated the main peak melting point temperature of PCM. The difference between temperature decreasing rates before and after the turning point was primarily due to the different liquid and solid PCMs' thermal conductivity, while the liquid PCM has greater thermal conductivity. The heat transfer mechanism throughout the discharging process shows heat conduction dominance as all the PCM temperatures changed in parallel and smoothly.

4.2. Study of energy savings of the thermoelectric cooling system using PCM as heat storage

Experimental results above give a general view of thermoelectric cooling system integrated with PCM heat storage. In this section, the efficacy of PCM heat storage has been investigated through a comparison experimental study. Two separate thermoelectric cooling lab experiments have been conducted through outdoor air heat dissipation (mode 1) and using PCM heat storage (mode 2), respectively, with all other experimental conditions kept approximately the same. Both experiments lasted for a 2-h period and both experiments were applied the same electric current and voltage.

The lab room temperature was maintained at 30 ± 0.3 °C as shown in Fig. 13. The chamber temperature was controlled at 24 ± 0.3 °C through manual on/off control of the thermoelectric cooling system.

Fig. 13(a) presents experimental result of mode 1 while Fig. 13(b) is for mode 2. From Fig. 13(a), outdoor air temperature was relatively high during the experiment in the range of 30–33 °C. The thermoelectric cooling system only shut off for a 4-min break during the 2-h experiment in mode 1. In contrast, for the similar cooling requirement (i.e. cooling load) because the lab room temperature was maintained the same level across two experiments

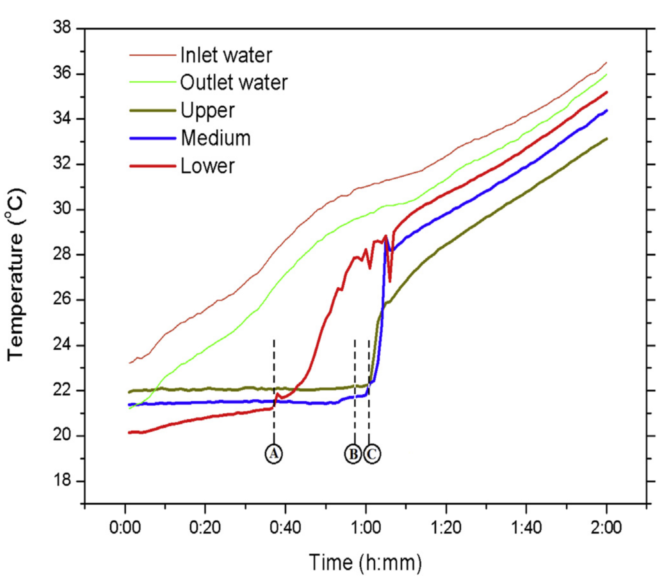

Fig. 11. Temperature variation of HTF and PCM during charging (melting) process.

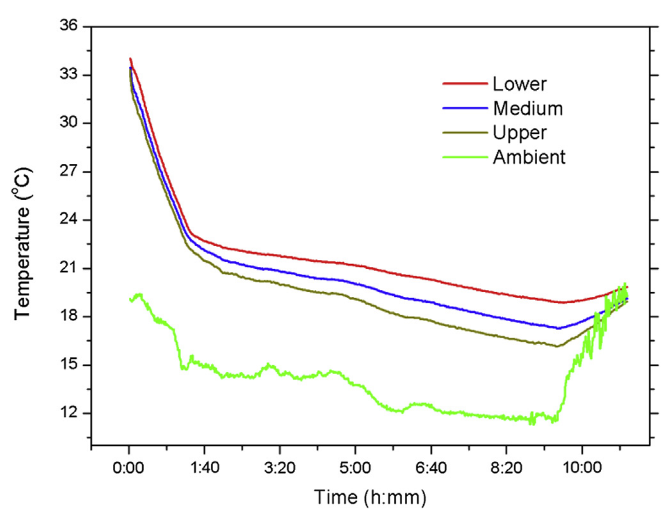

Fig. 12. Discharging (solidifying) process of the PCM at night.

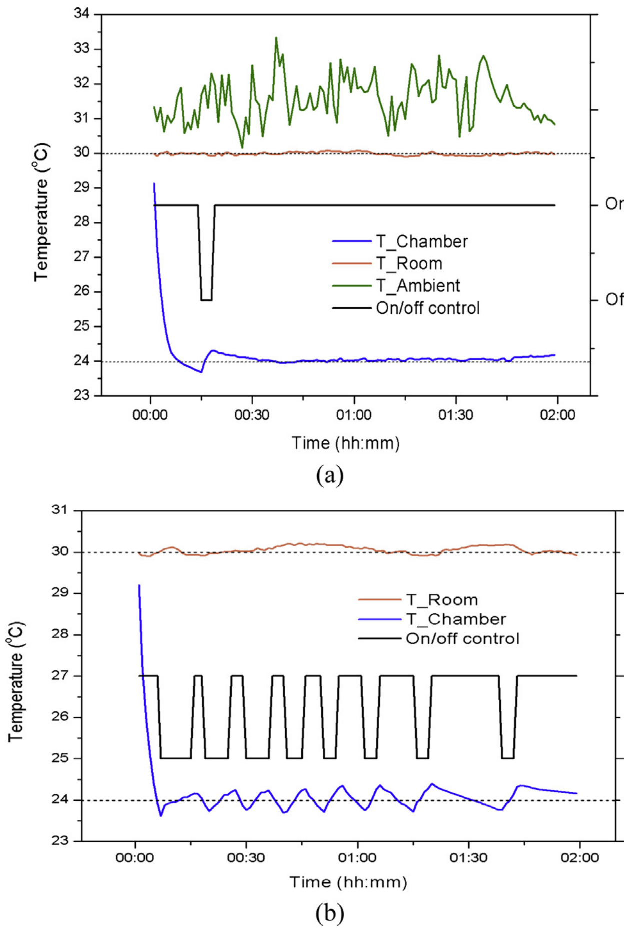

Fig. 13. Comparison experiments for thermoelectric cooling with heat dissipation to (a) outdoor ambient air (mode 1), and (b) PCM heat storage unit (mode 2).

more on/off switches have been applied with an observed zigzag type change for chamber air temperature during the experiment in mode 2 (see Fig. 13(b)). It also can be seen that cooling capability of the thermoelectric system with PCM heat storage gradually decreased because as time went by, it took longer for the thermoelectric cooling system to cool down the chamber.

When experiments finished, the cooling system's running time has been added together for each experiment and obtained 116 and 75 min for mode 1 and mode 2 experiments, respectively. Since the input electric current and voltage were kept the same during the entire experiment for both experiments, the electric power usage should be proportional to the system's total running time. Therefore, the energy savings can be estimated and an approximate 35.3% of electrical energy has been saved through using the PCM heat storage unit from the comparison experiments.

An alternative approach to show the efficacy of PCM heat storage is through using the effective cooling COP (COP_{eff}) for the entire experiment, which is defined in Eq. (13) using total cooling power achieved (Q_t) divided by total electrical power input (P_t).

Table 4
Uncertainty analysis for measured variables.

Variable	Typical value (x)	Uncertainty (δx)	Relative uncertainty ($\delta x/x$)
$T_{\_Room}$ (°C)	30	0.2	0.67%
$T_{\_Chamber}$(°C)	22–30	0.1	0.45%
$T_{\_Ambient}$(°C)	30–33	0.1	0.33%
$T_{\_PCM}$ (°C)	20–35	0.1	0.5%
$T_{\_air,\ inlet}$ (°C)	20–30	0.1	0.5%
$T_{\_air,\ outlet}$ (°C)	15–30	0.1	0.67%
U (V)	0–30	–	0.5%
I (A)	0–5	–	1%
$V_{\_air}$ (m/s)	2–3	0.1	5%

$$\mathrm{COP_{eff}} = \frac{Q_t}{P_t} = \frac{\sum (Q_{\mathrm{unit}})_i \Delta t_i}{\sum (nP_{\mathrm{mod}})_i \Delta t_i} \tag{13}$$

From this definition, the effective cooling COPs in the 2-h experiments for mode 1 and mode 2 have been calculated and the results are 0.50 and 0.78, respectively. Without PCM heat storage, the effective COP of the 2-h experiment for mode 1 was 0.50, which shows comparable performance efficiency as other researches [5,7]. But with PCM heat storage, the system's effective COP value increased to 0.78, which demonstrates the important contribution of the PCM heat storage when integrating with the thermoelectric cooling system.

4.3. Uncertainty analysis and reproducibility of the experiment results

All the temperature measurements in the experiments were conducted by using pre-calibrated T-type thermocouples with an accuracy of ±0.1 °C. Air velocity measurements have been completed using EA-3010U anemometer which has a resolution of ±0.1 m/s. Average values of air velocity and temperature were obtained through 10 measuring points at the air inlet and outlet cross-section of the thermoelectric cooling unit for computing cooling capacity. A TP4000ZC digital multi-meter was used to measure the voltage with 0.5% accuracy and the current with 1.0% accuracy.

When the uncertainties in measured quantities were estimated and tabulated in Table 4, the overall uncertainty analysis for calculated quantities was accomplished through using the RSS (root-sum-squares) method described by Moffat [32]. The uncertainty of each calculated variables was estimated with 95% confidence. The uncertainty analysis of cooling COP was presented as an example in Eq. (14). The relative uncertainty of cooling COP was estimated within the range of 1.3%–2.6%.

As shown in Table 4, the temperature, air velocity, and electrical power measurements were accurate and reliable in the experiments. However, regarding the reproducibility of experimental results, deviation may be introduced particularly by the variations of the outdoor air temperature and initial temperature distribution within the PCM heat storage as these two temperatures were not precisely controlled in this study. If the average outdoor air temperature for mode 1 and average PCM initial temperature for mode 2 would be maintained in future experiments, the deviation shall be limited.

$$\delta COP_c = \sqrt{\sum_{i=1}^{n}\left(\frac{\partial COP_c}{\partial T_{\mathrm{air,outlet}}}\delta T_{\mathrm{air,outlet}}\right)^2 + \sum_{i=1}^{n}\left(\frac{\partial COP_c}{\partial T_{\mathrm{air,inlet}}}\delta T_{\mathrm{air,inlet}}\right)^2 + \sum_{i=1}^{n}\left(\frac{\partial COP_c}{\partial V_{\mathrm{air}}}\delta V_{\mathrm{air}}\right)^2 + \left(\frac{\partial COP_c}{\partial U}\delta U\right)^2 + \left(\frac{\partial COP_c}{\partial I}\delta I\right)^2} \tag{14}$$

5. Conclusions

To enhance thermoelectric cooling system's efficiency in space cooling application, a prototype thermoelectric cooling system integrated with PCM heat storage has been introduced in this paper. Performance of the thermoelectric modules has been analyzed using a simplified analytical model, and the results from evaluating modules' theoretical performance provided balance between the cooling efficiency and capacity for setting-up experimental operations. Experiments have been conducted to evaluate the thermoelectric cooling system's performance and comparison experimental study has been used to show the efficacy of PCM heat storage in terms of energy savings and effective COP. The following conclusions can be obtained from the study:

- For a 2-h chamber cooling experiment, the thermoelectric cooling system's average COP has been found being 0.87, with a maximum COP value of 1.22. The air temperature difference between the chamber (representing a model room) and the lab room (representing outdoor environment) on average was about 7 °C. The maximum cooling capacity achieved was 210 W.
- Natural convection during PCM charging (melting) process has a noticeable effect on heat transfer in PCM, especially in the melting stage when there is a large temperature difference inside the PCM.
- Comparison experimental study showed that 35.3% electrical energy has been saved in the prototype thermoelectric cooling system through using PCM heat storage under the condition that outdoor air temperature was in the range of 30–33 °C and the conditioned space was set for being cooled at 24 °C.

This PCM heat storage system is a short-term diurnal thermal storage application, which is suitable for areas that have large temperature differences between day and night. For future's specific cooling application, the volume of PCM (or total heat storage capacity) needed should be computed according to the cooling load and weather condition. Moreover, for system's flexible operation, the PCM charging speed should be controllable using the HTF circulation pump. Besides integrating with thermoelectric cooling system, this PCM integrated approach can be applied to other systems such as the conventional air-conditioners. The thermoelectric module used in this work has a figure-of-merit ZT value of only 0.74. If the ZT factor of the thermoelectric material could be further improved and increased to, for example, 2.0 in the next decade, the COP value and energy saving of this thermoelectric cooling system could be further increased.

References

[1] Bell LE. Cooling, heating, generating power, and recovering waste heat with thermoelectric systems. Science 2008;321:1457–61.
[2] Vining CB. An inconvenient truth about thermoelectrics. Nat Mater 2009;8: 83–5.
[3] Dresselhaus MS, Chen G, Tang MY, Yang R, Lee H, Wang D, et al. New directions for low-dimensional thermoelectric materials. Adv Mater 2007;19: 1043–53.
[4] Snyder GJ, Toberer ES. Complex thermoelectric materials. Nat Mater 2008;7: 105–14.
[5] Gillott M, Jiang L, Riffat SB. An investigation of thermoelectric cooling devices for small-scale space conditioning applications in buildings. Int J Energy Res 2010;34:776–86.
[6] Cheng TC, Cheng CH, Huang ZZ, Liao GC. Development of an energy-saving module via combination of solar cells and thermoelectric coolers for green building applications. Energy 2011;36:133–40.
[7] He W, Zhou J, Hou J, Chen C, Ji J. Theoretical and experimental investigation on a thermoelectric cooling and heating system driven by solar. Appl Energy 2013;107:89–97.
[8] Shen L, Xiao F, Chen H, Wang S. Investigation of a novel thermoelectric radiant air-conditioning system. Energy Build 2013;59:123–32.
[9] Miranda AG, Chen TS, Hong CW. Feasibility study of a green energy powered thermoelectric chip based air conditioner for electric vehicles. Energy 2013;59:633–41.
[10] Riffat SB, Qiu G. Comparative investigation of thermoelectric air-conditioners versus vapour compression and absorption air-conditioners. Appl Therm Eng 2004;24:1979–93.
[11] Hermes CJL, Barbosa JR. Thermodynamic comparison of Peltier, Stirling, and vapor compression portable coolers. Appl Energy 2012;91:51–8.
[12] Riffat SB, Ma X. Improving the coefficient of performance of thermoelectric cooling systems: a review. Int J Energy Res 2004;28:753–768,.
[13] Min G, Rowe DM. Experimental evaluation of prototype thermoelectric domestic-refrigerators. Appl Energy 2006;83:133–52.
[14] Abdul-Wahab SA, Elkamel A, Al-Damkhi AM, Al-Habsi IA, Al-Rubai'ey' HS, Al-Battashi AK, et al. Design and experimental investigation of portable solar thermoelectric refrigerator. Renew Energy 2009;34:30–4.
[15] Wang CC, Hung CI, Chen WH. Design of heat sink for improving the performance of thermoelectric generator using two-stage optimization. Energy 2012;39:236–45.
[16] Naphon P, Wiriyasart S. Liquid cooling in the mini-rectangular fin heat sink with and without thermoelectric for CPU. Int Commun Heat Mass Transf 2009;36:166–71.
[17] Zhang HY, Mui YC, Tarin M. Analysis of thermoelectric cooler performance for high power electronic packages. Appl Therm Eng 2010;30:561–8.
[18] Vian JG, Astrain D. Development of a thermoelectric refrigerator with two-phase thermosyphons and capillary lift. Appl Therm Eng 2009;29:1935–40.
[19] Vian JG, Astrain D. Development of a heat exchanger for the cold side of a thermoelectric module. Appl Therm Eng 2008;28:1514–21.
[20] Wang X, Yu J, Ma M. Optimization of heat sink configuration for thermoelectric cooling system based on entropy generation analysis. Int J Heat Mass Transf 2013;63:361–5.
[21] Rowe DM, editor. Thermoelectrics handbook: macro to nano. CRC Taylor & Francis Group; 2006.
[22] Lee H. Optimal design of thermoelectric devices with dimensional analysis. Appl Energy 2013;106:79–88.
[23] Chen M, Snyder GJ. Analytical and numerical parameter extraction for compact modeling of thermoelectric coolers. Int J Heat Mass Transf 2013;60: 689–99.
[24] Reddy BVK, Barry M, Li J, Chyu MK. Mathematical modeling and numerical characterization of composite thermoelectric devices. Int J Therm Sci 2013;67: 53–63.
[25] Mitrani D, Salazar J, Turo A, Garcia MJ, Chavez JA. One-dimensional modeling of TE devices considering temperature-dependent parameters using SPICE. Microelectron J 2009;40:1398–405.
[26] Cheng CH, Huang SY, Cheng TC. A three-dimensional theoretical model for predicting transient thermal behavior of thermoelectric coolers. Int J Heat Mass Transf 2010;53:2001–11.
[27] Meng JH, Wang XD, Zhang XX. Transient modeling and dynamic characteristics of thermoelectric cooler. Appl Energy 2013;108:340–8.
[28] Meng JH, Zhang XX, Wang XD. Dynamic response characteristics of thermoelectric generator predicted by a three-dimensional heat-electricity coupled model. J Power Sources 2014;245:262–9.
[29] Technical data sheet for RC12-8. Marlow Industries, Inc.
[30] Huang YX, Wang XD, Cheng CH, Lin DT. Geometry optimization of thermoelectric coolers using simplified conjugate-gradient method. Energy 2013;59: 689–97.
[31] Wang XD, Huang YX, Cheng CH, Lin DT, Kang CH. A three-dimensional numerical modeling of thermoelectric device with consideration of coupling of temperature field and electric potential field. Energy 2012;47:488–97.
[32] Moffat RJ. Describing the uncertainties in experimental results. Exp Therm Fluid Sci 1988;1:3–17.